

Measurement of the electron-pressure profile of galaxy clusters in Wilkinson Microwave Anisotropy Probe (WMAP) 3-year data.

F. Atrio-Barandela^{1,5}, A. Kashlinsky², D. Kocevski³, H. Ebeling⁴

ABSTRACT

Using WMAP 3-year data at the locations of close to ~ 700 X-ray selected clusters we have detected the amplitude of the thermal Sunyaev-Zeldovich (TSZ) effect at the 15σ level, the highest statistical significance reported so far. Owing to the large size of our cluster sample, we are able to detect the corresponding CMB distortions out to large cluster-centric radii. The region over which the TSZ signal is detected is, on average, four times larger in radius than the X-ray emitting region, extending to $\sim 3h_{70}^{-1}\text{Mpc}$. We show that an isothermal β model does not fit the electron pressure at large radii; instead, the baryon profile is consistent with the Navarro-Frenk-White profile, expected for dark matter in the concordance ΛCDM model. The X-ray temperature at the virial radius of the clusters falls by a factor $\sim 3 - 4$ from the central value, depending on the cluster concentration parameter. Our results suggest that cluster dynamics at large radii is dominated by dark matter and is well described by Newtonian gravity.

Subject headings: Cosmic Microwave Background. Cosmology: theory. Cosmology: observations.

1. Introduction.

The hot intergalactic X-ray emitting gas distorts the Cosmic Microwave Background (CMB) spectrum of those photons crossing the cluster. The CMB distortions are independent

¹Física Teórica, Universidad de Salamanca, 37008 Salamanca, Spain

²SSAI and Observational Cosmology Laboratory, Code 665, Goddard Space Flight Center, Greenbelt MD 20771

³Department of Physics, University of California at Davis, 1 Shields Avenue, Davis, CA 95616

⁴Institute of Astronomy, University of Hawaii, 2680 Woodlan Dr, Honolulu, HI 96822

⁵e-mail: atrio@usal.es

of redshift and arise from Thompson scattering; when electrons are non-relativistic, they are caused by two different effects: (1) the Thermal Sunyaev-Zel'dovich effect (TSZ, Sunyaev & Zel'dovich 1972) is due to the thermal motions of electrons in the cluster potential well, whereas (2) the Kinematic Sunyaev-Zel'dovich effect (KSZ) is due to the motion of the cluster as a whole. Both effects contribute to the CMB radiation power spectrum, but their contribution is significant at $\ell > 10^3$ (Atrio-Barandela & Mücke 1999, Molnar & Birkinshaw 2000). For the most luminous clusters, relativistic corrections could become important, giving rise to the relativistic SZ effect (Wright, 1979). The TSZ spectral signature appears as a temperature decrement in the WMAP frequency range. It has been measured for ~ 100 individual clusters (Birkinshaw 1998, Carlstrom, Holder & Reese 2002, LaRoque et al 2007), while the KSZ effect, being of much smaller amplitude, has not yet been detected for individual systems. It can, however, be detected statistically with large cluster samples (Kashlinsky & Atrio-Barandela, 2000) using a method recently applied by us to measure the bulk motion of clusters on scales out to $\sim 300h^{-1}\text{Mpc}$ (Kashlinsky et al 2007).

Currently planned ground- and space-borne CMB experiments like the South Pole Telescope, the Atacama Cosmology Telescope and the PLANCK mission are expected to detect clusters via their TSZ signature in the near future. In the meantime, first efforts to determine the TSZ contribution to the CMB fluctuations observed by WMAP across the entire sky (Spergel et al 2007) were made by cross-correlating templates constructed from galaxy and cluster catalogs using 1st-year data (Hernández-Monteagudo & Rubiño Martín 2004, Hernández-Monteagudo, Génova-Santos & Atrio-Barandela 2004, Myers et al 2004, Afshordi, Lin & Sanderson 2005) and, more recently, 3rd-year data (Afshordi et al 2007). These studies report $2-8\sigma$ detections of an anti-correlation with various galaxies and cluster surveys, consistent with the expected TSZ signature at WMAP frequencies.

A more efficient detection of the SZ effect is possible by examining the WMAP data at the location of X-ray detected clusters since both the SZ and the X-ray data probe the same hot ICM. In this letter, we use the largest to-date all-sky cluster catalog, containing 782 clusters with well measured X-ray parameters from ROSAT All-Sky Survey data (RASS, Voges et al 1999), to determine the TSZ amplitude present in the WMAP 3yr data and to evaluate the properties of the cluster SZ signal. We describe in Sec. 2 the catalog and WMAP data, present our results in Sec. 3, and discuss their implications in Sec. 4.

2. X-ray catalog and CMB data

Our analysis uses an all-sky cluster sample created by combining the ROSAT-ESO Flux Limited X-ray catalog (REFLEX, Böhringer et al 2004) in the southern hemisphere, the

extended Brightest Cluster Sample (eBCS, Ebeling et al 1998, Ebeling et al 2000) in the north, and the Clusters in the Zone of Avoidance (CIZA, Ebeling, Mullis & Tully 2002, Kocevski et al 2007) sample along the Galactic plane. All three surveys are X-ray selected and X-ray flux limited using RASS data. A detailed description of the creation of the merged catalog is provided by Kocevski & Ebeling (2006).

For each cluster, the catalog lists position, flux, and luminosity measured directly from RASS data; X-ray electron temperature, derived from the $L_X - T_X$ relation of White, Jones & Forman (1997), redshifts, and angular and physical extent of the region containing the measured X-ray flux. We determine the X-ray extent of each cluster directly from the RASS imaging data using a growth-curve analysis. The cumulative profile of the net count rate is constructed for each system by measuring the counts in successively larger circular apertures centered on the X-ray emission and subtracting an appropriately scaled X-ray background. The latter is determined in an annulus from 2 to 3 h_{50}^{-1} Mpc around the cluster centroid. The extent of each system is then defined as the radius at which the increase in the source signal is less than the 1σ Poissonian noise of the net count rate.

To obtain an analytic parametrization of the spatial profile of the X-ray emitting gas and, ultimately, the central electron density we fit a β model (Cavaliere & Fusco-Femiano 1976) convolved with the RASS point-spread function to the RASS data for each cluster in our sample: $S(r) = S_0 [1 + (r/r_c)^2]^{-3\beta+1/2}$ where $S(r)$ is the projected surface-brightness distribution and S_0 , r_c , and β are the central surface brightness, the core radius, and the β parameter characterising the profile at large radii. Using the results from this model fit to determine the gas-density profile assumes the gas to be isothermal and spherically symmetric. In practice, additional uncertainties are introduced by the correlation between r_c and β which makes the results for both parameters sensitive to the choice of radius over which the model is fit, and the fact that for all but the most nearby clusters the angular resolution of the RASS allows only a very poor sampling of the surface-brightness profile (at $z > 0.2$ the X-ray signal from a typical cluster is only detected in perhaps a dozen RASS image pixels). In recognition of these limitations, we hold β fixed at the canonical value of $2/3$ (Jones & Forman, 1984). The resulting values for r_c are reassuringly robust in the sense that we find broad agreement with the empirical relationship between X-ray luminosity and r_c determined by Reiprich & Böhringer (1999). Our best-fit parameters, the cluster luminosity and electron temperature, are used to determine central electron densities for each cluster using Eq. (6) of Henry & Henriksen (1986) with the ICM temperature estimated from the $L_X - T_X$ relationship (White et al 1997). Other sources of error of this parametrization, namely the deviation from a β profile at small radii due to cooling cores as well as the steepening of the profile often observed at large radii (Vikhlinin, Forman & Jones, 1999) are unlikely to affect our results due to the poor resolution and low signal-to-noise of

the RASS data. Conversions between angular extents and the physical dimensions of clusters are made using the Λ CDM concordance cosmology ($\Omega_\Lambda = 0.7$, $h = 0.7$).

In our analysis of the CMB data, we use maps from eight differencing assemblies (DA) corresponding to the Q, V and W bands of the “foreground-cleaned” WMAP 3-year data: Q1, Q2, V1, V2, W1,..., W4 available from the Lambda archive (<http://lambda.gsfc.nasa.gov>). We do not use the K and Ka bands since foreground contamination is important at those frequencies (Bennett et al 2003). The maps are written in the HEALPix (Gorski et al 2005) nested format with resolution $N_{side} = 512$, corresponding to pixels of $7'$ on the side, significantly larger than the $0.75'$ pixels of the X-ray data, which makes our results insensitive to deviations from spherical symmetry of the clusters in our sample. These bands correspond to frequencies 41, 61, and 94 GHz and angular resolutions $\theta_{FWHM} \simeq 0.5, 0.3$, and 0.2 degrees. All maps are multiplied by the Kp0 mask to remove microwave emission from the Galactic plane and foreground sources. The masking eliminates 120 clusters, leaving 674 clusters for our SZ analysis. Of those, 13 clusters did not have sufficient S/N in the ROSAT data to define an extent and were excluded from this analysis leaving a total of 661 clusters.

3. Results.

To compute the TSZ signal from the WMAP 3-year data we evaluate the mean temperature anisotropy at the cluster locations. The TSZ distortion scales as the electron density, n_e , integrated along the line-of-sight, whereas the cluster X-ray emission is $\propto n_e^2$. Thus, the clusters' SZ signal should extend over an area significantly larger than the region within which X-ray emission is detectable. We probe the SZ extent by measuring the signal in regions of increasing radius θ_{SZ} , from 1 to $6\theta_X$, where θ_X is the angular extent of the respective cluster in the RASS data. The results from the individual DA's were averaged with weights inversely proportional to the pixel noise and the frequency-dependent amplitude of the SZ effect, and without weights. The difference between the results obtained with the different weighting schemes are smaller than 5% and we quote results obtained using noise and frequency-weighted averages. Error bars are calculated assigning 1,000 random pseudo-cluster positions to the WMAP sky and computing the mean temperature anisotropy for each cluster template. The random positions are always placed outside the Kp0 mask and away from any of the cluster pixels.

In Table 1 we present our results for two subsamples: clusters with redshift $z \leq 0.2$ and clusters with luminosity $L_X([0.1 - 2.4]\text{keV}) \geq 3 \times 10^{44}\text{erg/s}$. The limit of $z = 0.2$ was chosen since this is the largest redshift out to which our cluster catalog is reasonably complete. We use the average values of the core radii and radial cluster extent for each

subsample. The TSZ signal is measured within (a) a disc of angular radius θ , and (b) a ring or annulus delimited by two consecutive discs, to differentiate the contribution coming from regions increasingly farther away from the cluster core. By design, the first DISC and RING regions are identical. We measure a temperature decrement at the cluster pixels at the $\sim 15\sigma$ level for the most X-ray luminous clusters. The region from 3-4 times the X-ray extent still shows a non-negligible contribution, while outside this region no statistically significant signal is detected. The average radius of the regions contributing to the signal is $\simeq 2 - 3h_{70}^{-1}\text{Mpc}$, depending on the cluster sample. The fact that clusters appear more extended at microwave than at X-ray frequencies was used by us (Kashlinsky et al 2008) to isolate the KSZ component arising from the cluster bulk motion; as we demonstrate below the cluster X-ray temperature decreases towards cluster outskirts making the KSZ dipole appear still more extended than the TSZ contributions.

In Fig. 1 we show the TSZ amplitude for different cluster subsamples and regions of different radius. In Fig. 1a, we plot the results for clusters within a progressively increasing upper redshift limit; the last data point includes all clusters. Except for the lowest redshift bins the measured amplitude is roughly independent of the number of clusters. In Fig. 1b we show the frequency dependence of the measured TSZ signal for all clusters with redshift $z \leq 0.2$ by comparing the result for the three bands considered: Q, V, and W. Solid lines denote the frequency dependence of the TSZ effect with the curves normalized by least squares regression. Note that for the smallest angular extent the TSZ signal shows frequency spectrum which differs significantly from the TSZ expectation. Earlier analysis by Hernández-Monteagudo et al (2004) also did not find a clear TSZ scaling in WMAP 1st-year data. This difference could originate due to the different angular resolution and noise levels between the Q, V and W bands. Due to its smaller resolution, the Q channel probes the SZ decrement to a larger extent and dilutes the central SZ amplitude more than in the V or W bands. As we include the contribution from progressively larger radii the effect of noise and resolution is reduced; by the time we reach $\theta_{\text{SZ}} = 4 - 6\theta_X$, the change in frequency at the 3 bands agrees very well with the spectral dependence of the TSZ effect. Other components have negligible contribution. A bulk flow motion will give rise to a dipole pattern but does not change the monopole evaluated at cluster locations. In the Rayleigh-Jeans regime, the first correction to the TSZ frequency scaling due to the relativistic effect is $1.7(k_B T_X / m_e c^2)$ (see Itoh, Kohyama & Nozawa, 1998). The average temperature of all clusters in our catalog is $k_B T_X \sim 4\text{KeV}$, so the relativistic correction represents less than a 1.4% variation. Dashed and dot-dashed lines in Fig. 1b represent the frequency dependence of the KSZ and relativistic SZ effect, the latter computed using the approximate solution of Itoh et al (1998) for a cluster of $k_B T_X = 10\text{KeV}$, arbitrarily normalized to the amplitude of the V-band.

The radial emission profiles derived from SZ and X-ray observations of clusters do

not necessarily follow the same β model. Only a handful of clusters have measured radial SZ profiles and the parameters obtained from X-ray data are often used in SZ analysis. Using numerical simulations, Hallman et al (2007) showed that this approach leads to biased estimates of the integrated Compton y -parameter in the inner part of clusters. Since we measure the TSZ contribution outside the inner cluster region, we can test for a similar bias in the outskirts of clusters and assess the accuracy of the β model. In Fig. 2 a comparison is made between our measured radial SZ profile (full circles, see also Table 1) and β model predictions (diamonds). Predictions are computed with the same pipeline as the data from the eight DA maps generated by placing clusters on the sky with their measured angular size. To each pixel within a cluster we assign CMB temperature derived from the β model TSZ profile, convolved with the WMAP beam for each DA. The angular scale θ_{SZ} is the area weighted average extent of cluster.

The discrepancy between data and the $\beta = 2/3$ prediction is less than a few μK or 10 – 30% in the cluster centers, but increases with radius and reaches a factor of 2 – 3 at the largest radius probed in our study. It could be argued that a model with $\beta = 1$ would fit the data in the cluster outskirts. Such a high β value would not only invalidate the values of r_c and n_c derived directly from the RASS X-ray data, it would in fact be inconsistent with the shape of the X-ray surface brightness profile in the central region of essentially every cluster ever observed. Jones and Forman (1999) found that the average cluster surface-brightness profile is well described by a β model with $r_c \sim 200\text{Kpc}$ and $\beta \sim 0.6$. Out of 96 clusters analyzed in detail, they did not find a single one for which a β value outside the range of 0.4–0.8 would provide an acceptable fit to the X-ray data.

Numerical hydrodynamic simulations suggest that the dark-matter distribution in galaxy clusters is described by a universal density profile (Navarro, Frenk & White 1997, NFW), $\rho_{dm}(x) = \rho_s/[x(1+x)^2]$, where $x = r/r_s$, r_s and ρ_s are a characteristic scale radius and density. Usually r_s is given in terms of the concentration parameter $c = r_v/r_s$ where r_v is the halo virial radius. This parameter depends only weakly on mass, with less massive systems being more concentrated, having larger c . While the electron density for the $\beta = 2/3$ model scales as r^{-2} at large radii, the NFW is much steeper, scaling as r^{-3} . If the gas distribution were to follow that of the dark matter, one would thus expect its radial profile to decline much more steeply, as observed and shown in Fig. 2. Solid lines represent the electron pressure profile of a single cluster computed using a β (upper) and a NFW model (lower solid line), convolved with the WMAP 3-year beam. Our fits (β and NFW model alike) assume a representative cluster redshift of $z = 0.12$, a value close to the mean redshift of both cluster subsamples. The best-fit values for the core radius of the β model are $\theta_c = 1.5', 0.5'$ (a and b, respectively). We checked that no value of $r_c \in [0.5, 5]\text{arcmin}$ can make the β model fit the measured pressure profile. To generate the NFW profile, we follow

Komatsu & Seljak (2001, 2002) and assume that the gas follows the DM distribution, is in hydrostatic equilibrium, and is well described by a polytropic equation of state. Fitting an NFW model yields best-fit concentration parameters of $c = 8$ (a) and $c = 15$ (b). In the Komatsu & Seljak (2001) model, these values correspond to polytropic indices $\gamma = 1.17, 1.2$, respectively. This result reflects that the most luminous clusters are, on average, further away in a flux limited sample than the whole population, so they subtend a smaller angular size and appear concentrated (smaller r_s in NFW) or have a smaller core radius (in the β model). In Fig. 2, theoretical lines represent the TSZ signal of a single cluster; as such, they are not a fair representation of the cluster population as a whole. If θ_{SZ} were not the area weighted extent but the SZ emission weighted center, the best fit NFW and β models -solid lines in the figure- would correspond to slightly different model parameters but it will not change the discrepancy between the measured and the β model predicted profiles.

The universal gas temperature profiles of Komatsu & Seljak (2001), compatible with our results, show a strong decline of gas X-ray temperature with radius. The central temperature decreases by a factor 2-4 at the virial radius, being steeper for the more concentrated (less massive) clusters. This result is in agreement with the recent analysis of X-ray temperature profiles of 15 nearby clusters, carried out by Pratt et al (2007) using XMM-Newton data. They measured temperature profiles declining by a factor ~ 2 at half the virial radius, in good agreement with numerical simulations outside the core region. To conclude, Fig. 2 shows that the gas density has a steeper decline in the outer region than an isothermal $\beta = 2/3$ model; the slope is close to -3, i.e., the dynamical state of cluster outskirts is well described by a NFW profile.

4. Conclusions.

Using the largest X-ray cluster catalog available today we present an accurate measurement of the contribution of clusters of galaxies to the temperature anisotropies measured by the WMAP satellite in its three-year data release. We find the TSZ signal to extend to, on average, $\sim 2 - 3h_{70}^{-1}\text{Mpc}$, i.e., radii much larger than the ones out to which X-ray emission is detectable. The TSZ signal measured in the cluster cores shows deviations the expected TSZ frequency behavior. These are likely caused by the different angular resolution of the WMAP Q, V, W channels resulting in probing SZ decrement from different parts of the clusters. However, when the TSZ contribution from the outer cluster regions is included, the signal is consistent with the frequency dependence of a TSZ spectrum.

The measurement indicate that the gas profile of the cluster population in the outer region is compatible with the NFW model. Our results suggests than the cluster temperature

profile declines with radius, in agreement with numerical simulations of clusters and recent XMM data. We are currently rederiving the NFW data parameters from the X-ray images to compare the TSZ predicted for the cluster population using X-ray derived quantities with the signal at WMAP frequencies. The radial profile of the measured TSZ signal suggests that, all the way to the cluster outskirts, baryons are settled in hydrostatic equilibrium within the DM potential well and follow the same density distribution. As shown by numerical simulations, the profile of collapsed dark matter haloes is a direct consequence of the Newtonian gravity with a suitably chosen initial density field (corresponding to the concordance Λ CDM model). Hence our results also provide further, albeit indirect, evidence for the existence of dark matter and the validity of the Newtonian dynamics.

This work is supported by the Ministerio de Educación y Ciencia and the "Junta de Castilla y León" in Spain (FIS2006-05319, PR2005-0359 and SA010C05) and by NASA ADP grant NNG04G089G. We thank Gary Hinshaw for useful information regarding the WMAP data specifics. FAB thanks the University of Pennsylvania for its hospitality when part of this work was carried out.

REFERENCES

- Afshordi, N., Lin, Y.-T. & Sanderson, A.J.R. (2005), *ApJ*, 629, 1
- Afshordi, N., Lin, Y.-T., Nagai, D. & Sanderson, A.J.R. (2007) *MNRAS*, 378, 293
- Atrio-Barandela, F. & Mücke, J. (1999) *ApJ* 515, 465
- Bennett, C. et al (2003) *Ap.J. Suppl.*, 148,1
- Birkinshaw, M. (1998) *Physics Reports*, 310, 97
- Böhringer, H. et al. (2004) *A&A*, 425, 367
- Carlstrom, J.E., Holder, G.P., Reese, E.D. (2002) *ARAA*, 40, 643
- Cavaliere, A. & Fusco-Femiano, R. (1976) *A&A*, 49, 137
- Ebeling, H., Edge, A.C., Böhringer, H., Allen, S.W., Crawford, C.S., Fabian, A.C., Voges, W. & Huchra, J.P. (1998) *MNRAS*, 301, 881
- Ebeling, H., Edge, A.C., Allen, S.W., Crawford, C.S., Fabian, A.C. & Huchra, J.P. (2000) *MNRAS*, 318, 333

- Ebeling, H., Mullis, C.R. & Tully, R.B. (2002) ApJ, 580, 774
- Hallman, E.J., Burns, J.O., Motl, P.M., Norman, M.L. (2007). Preprint arXiv:075.0531
- Gorski, K. et al 2005, Ap.J., 622, 759
- Henry & Henriksen (1986) ApJ 301, 689
- Hernández-Monteagudo, C. & Rubiño-Martín, J.A. (2004) MNRAS, 347, 403
- Hernández-Monteagudo, C., Génova-Santos, R., Atrio-Barandela, F. (2004) 613, L89
- Itoh, N., Kohyama, Y. & Nozawa, S. (1998) ApJ, 502, 7
- Jones, C., Forman, W. (1984) ApJ 276, 38
- Jones, C., Forman, W. (1999) ApJ 511, 65
- Kashlinsky, A. & Atrio-Barandela, F. 2000, Ap.J., 536, L67
- Kashlinsky, A., Atrio-Barandela, F., Kocevski, D. & Ebeling, H. (2007) Nature, *submitted*.
- Kocevski, D.D. & Ebeling, H. (2006) ApJ, 645, 1043
- Kocevski, D.D., Ebeling, H., Mullis, C.R. & Tully, R.B. (2007) ApJ 662, 224
- Komatsu, E. & Seljak, U. (2001) MNRAS, 327, 1353
- Komatsu, E. & Seljak, U. (2002) MNRAS, 336, 1256
- LaRoque, S.J., Bonamente, M., Carlstrom, J.E., Joy, M.K., Nagai, D., Reese, E.D., Dawson, K.S. (2006)(2006) ApJ, 652, 917
- Monlar, S.M. & Birkinshaw, M. (2000) ApJ 537, 542
- Myers, A.D., Shanks, T., Outram, P.J., Frith, W.J. & Wolfendale, A.W. (2004) MNRAS 347, L67
- Navarro, J.F., Frenk, C.S. & White, S.D.M. (1997) ApJ, 490, 493
- Pratt, G.W., Boehringer, H., Croston, J.H., Arnaud, M., Borgani, S., Finoguenov, A., Temple, R.F. (2007) A& A, 461, 71
- Reiprich, T.H. & Böhringer, H. (1999) AN, 320, 296
- Spiegel, D. et al (2007) ApJS 170, 377

- Sunyaev, R.A. & Zel'dovich, Ya. B. 1972, Comments Astrophys. Space Phys., 4, 173
- Vikhlinin, A., Forman, W. & Jones, C. (1999) ApJ, 525, 47
- Voges, W. et al. (1999) A&AS, 349, 389
- White, D.A., Jones, C., Forman, W. (1997) MNRAS, 292, 419
- Wright, E.L. (1979) ApJ, 232, 348

$z_{cl} \leq 0.2$				$L_X \geq 3 \times 10^{44} \text{erg/s}$			
Data		TSZ (in μK)		Data		TSZ (in μK)	
θ/arcmin	r_{ext}/Mpc	Disc	Ring	θ/arcmin	r_{ext}/Mpc	Disc	Ring
(1)	(2)	(3)	(4)	(5)	(6)	(7)	(8)
4.4	0.6	-28.5 ± 2.3	-28.5 ± 2.3	4.0	1.0	-72.2 ± 4.8	-72.2 ± 4.8
8.8	1.3	-20.3 ± 1.8	-17.4 ± 2.0	8.0	1.9	-43.6 ± 3.7	-33.5 ± 4.2
13.2	1.9	-14.0 ± 1.6	-8.4 ± 2.1	12.0	2.9	-26.5 ± 3.2	-12.8 ± 4.3
17.4	2.5	-9.5 ± 1.4	-3.1 ± 2.1	16.0	3.8	-16.9 ± 2.9	-4.4 ± 4.4
21.7	3.1	-6.5 ± 1.3	-0.5 ± 2.1	20.0	4.8	-11.1 ± 2.6	-0.8 ± 4.3
25.8	3.8	-4.6 ± 1.2	0.4 ± 2.2	24.0	5.7	-8.2 ± 2.5	-1.7 ± 4.5

Table 1: TSZ amplitude evaluated at cluster locations for two cluster samples. Columns: (1,2,5,6) show the average angular and physical cluster radius for each subsample; (3,4,7,8) correspond to the measured TSZ signal in the WMAP-3yr data at the cluster locations. In DISC we measure the TSZ signal within a circle of angular radius $\theta_{\text{SZ}} = [1 - 6]\theta_X$, in RING within an annulus of width $1\theta_X$ and increasing radius.

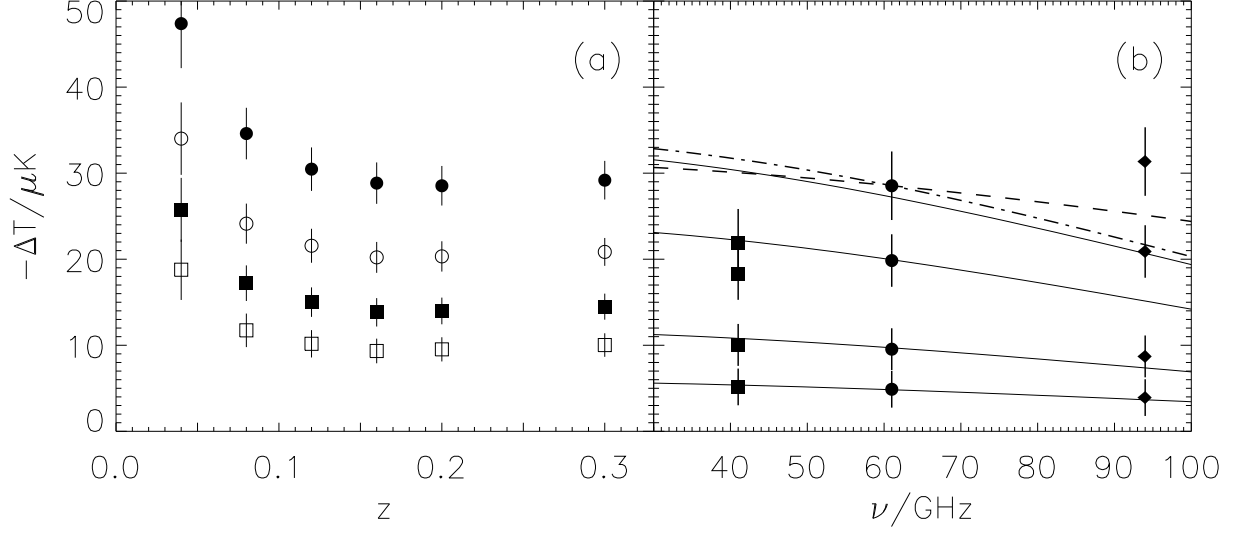


Fig. 1.— (a) TSZ signal in WMAP 3-year data for cluster subsamples with redshift $z \leq [0.04, 0.08, 0.12, 0.16, 0.2, 0.3]$. Close and open circles, squares and diamonds correspond to clusters with different angular extent. From top to bottom, the average was taken from clusters with total extent $\theta_{SZ} = (1 - 4) \times \theta_X$. (b) TSZ emission vs frequency is shown for different θ_{SZ} for: Q (squares), V (circles) and W (diamonds) bands and clusters with $z \leq 0.2$. Solid lines show the frequency dependence of the TSZ effect. From top to bottom $\theta_{SZ} = (1, 2, 4, 6) \times \theta_X$. In all cases, vertical bars indicate the 1σ errors. Curves were normalized by least squares regression. Dashed and dot-dashed lines show the frequency dependence of the KSZ and Relativistic SZ effects, respectively, normalized to the amplitude measured at the V-band.

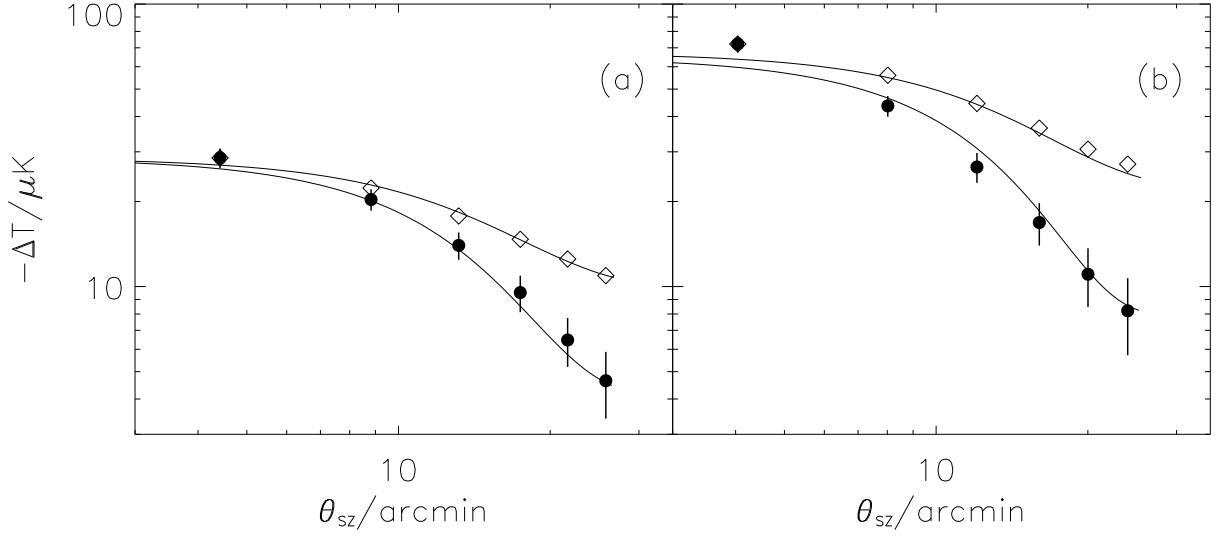


Fig. 2.— Measured and predicted electron pressure profile vs angular cluster-centric radius. Full circles and open diamonds correspond to the measured profile and the profile predicted for isothermal $\beta = 2/3$ model, respectively. Solid lines correspond to the β model (upper) and the NFW model fit (lower) assuming a single cluster at $z = 0.12$. We show results for two cluster subsamples: (a) $z \leq 0.2$, (b) $L_x[0.1 - 2.4 \text{ KeV}] \geq 3 \times 10^{44} \text{ ergs}^{-1}$. In (a) the best fit corresponds to $c = 8$ and $r_s = 350 h^{-1} \text{ kpc}$ and in (b) to $c = 15$ and $r_s = 250 h^{-1} \text{ kpc}$.